CHAPTER 4

Results

The observed images of the 11 sample galaxies have been analyzed and they had provided an information about their physical properties, i.e. masses, magnitudes, color indices, morphological types, $EW(\mathrm{H}\alpha + [\mathrm{N\,II}])$ and SFR. In order to interpret about interactions between the galaxies in NGC 4213 Group that affect on star formation activities and their evolution, the correlation among the properties were studied. Furthermore, the tidal interactions among galaxy-group and galaxy-galaxy clarified by the perturbation parameters were examined.

4.1 Colors and Magnitudes

After we obtained the apparent magnitudes in various broad-band filters from `GAIA` package, we get the color indices and calculate absolute magnitudes. They were plotted in three different diagrams, i.e. $B-V$, $B-R$, and $V-R$ versus B-band absolute magnitudes M_B, respectively.

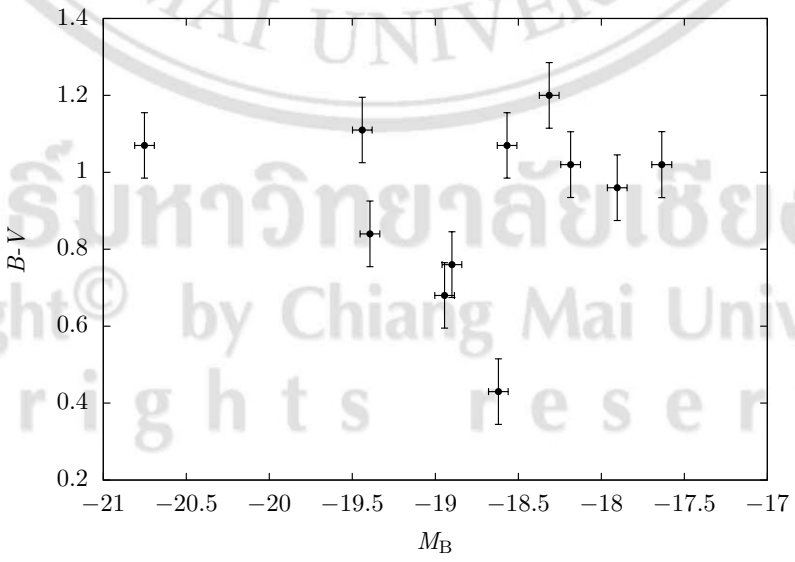

Figure 4.1: The diagram of B-V color against B-band absolute magnitudes.

The figure 4.1 to 4.3 display the relation between the color indices and absolute magnitudes. They were found that the brighter galaxies with low color index tend to be bluer than the fainter galaxies.

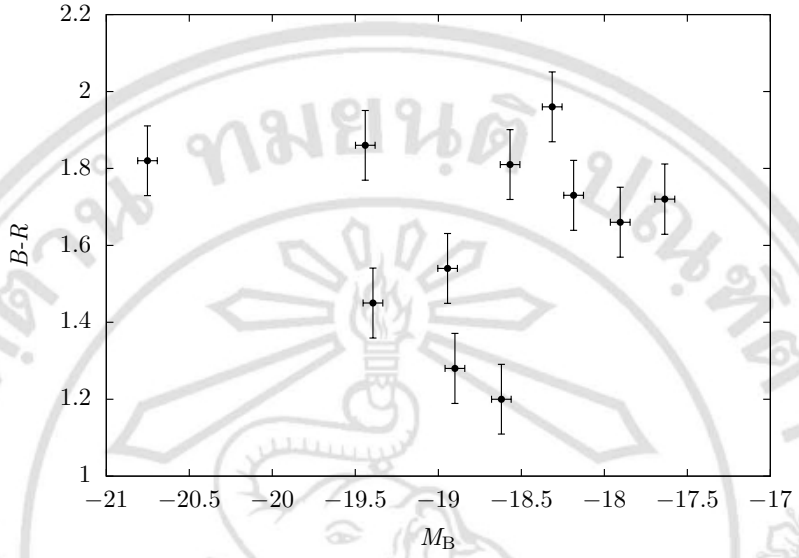

Figure 4.2: The diagram of B-R color against B-band absolute magnitudes.

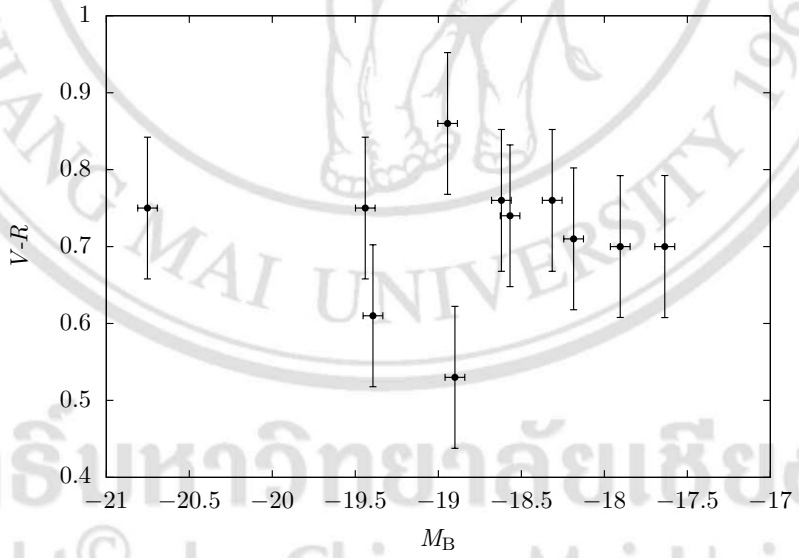

Figure 4.3: The diagram of V-R color against B-band absolute magnitudes.

These plots can be interpreted that the brighter galaxies might be consisted of higher proportion of blue stars. Commonly, blue stars are massive stars with high surface temperature that are recently formed. So the redder galaxies should be consisted of high fraction of cold, red, old stars and they have little or no star formation activities (Bennett et al.,

2012). Note that a galaxies with $M_{\rm B} = -20.752$ is more different value from other group members, because it is the greatest and brightest galaxy, while its color index is relatively high. In addition, this galaxies is classified as a early-type galaxy.

4.2 Color-T-type Relationship

Another part of the information we obtained from data images is the morphological types. The T-type of de Vaucouleurs system has been used to classify the morphology of the galaxies. $B - V$ color index was chosen to plot against the T-type. Figure 4.4 demonstrates the correlation between color and T-type.

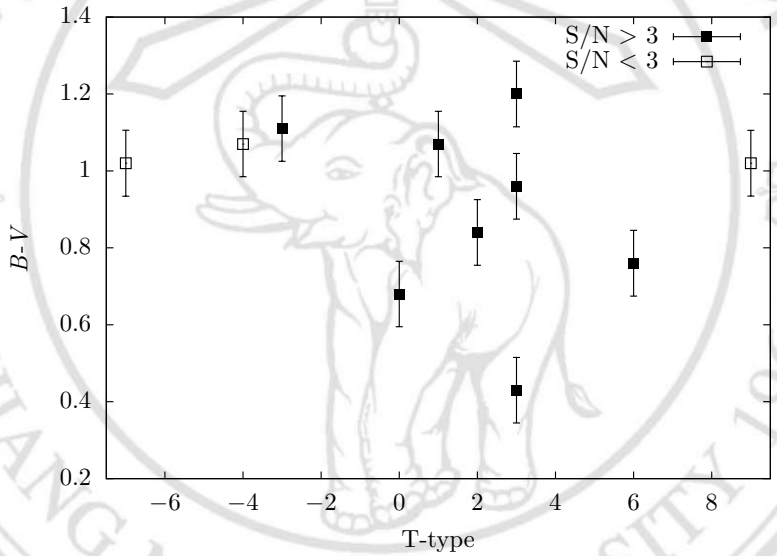

Figure 4.4: The $B - V$ color versus T-type diagram.

The galaxies with S/N of Hα flux counts more than 3 are designated by filled squares and the others are denoted by open squares. From the Hubble classification scheme and de vaucouleurs T-type, we define the galaxies for two main types, i.e. early-type (negative T-type) and late-type (positive T-type) galaxies. Likewise, the tend of the plot is analyzed for the color-T-type correlation. It was found that the late-type tend to be bluer than the early-type, this may be due to the late-type galaxies consist of relatively high proportion of hot, young, blue stars. In addition we can predict the late-type galaxies of this research contain much hydrogen gas which is the raw material for star formation. The star formation can be confirmed by the Hα + [N II] equivalent width in the next sections.

4.3 $H\alpha + [N\,II]$ Equivalent Width, Colors and T-types Relationships

Tracing of the star formation in the NGC 4213 Group galaxies can be carried out by detection of the $H\alpha + [N\,II]$ emission that emitted from the galaxies. $B - V$ color index and T-type were plotted against the $EW(H\alpha + [N\,II])$ as shown in figure 4.5 to 4.7.

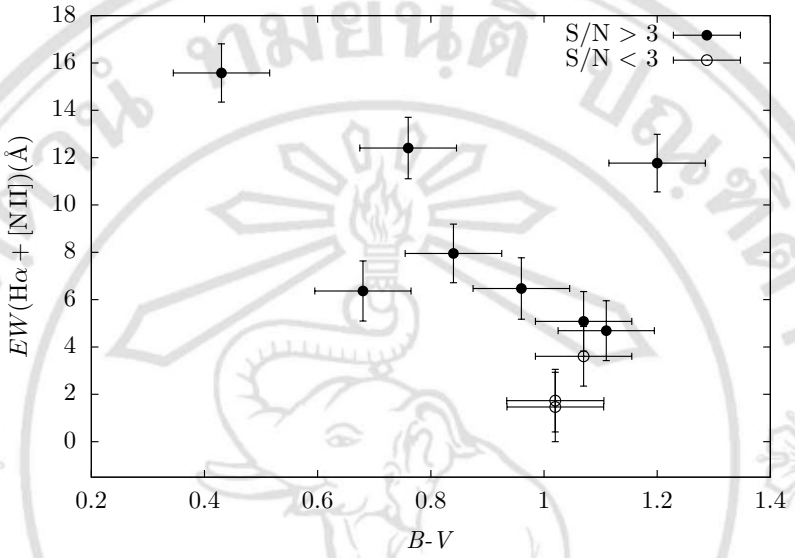

Figure 4.5: The diagram of $H\alpha + [N\,II]$ emission equivalent width against color indices of the galaxies.

From the figure 4.5, it was found that the bluer galaxies, the galaxies having less $B - V$ color index, tend to have high $EW(H\alpha + [N\,II])$ (Kennicutt and Kent, 1983). The highest $EW(H\alpha + [N\,II])$ is 15.577 Å, which is found in the blue galaxy with 0.431 $B-V$ color. Fossati et al. (2013) and Kennicutt (1998) mentioned that the $EW(H\alpha + [N\,II])$ could be the indicator for star-forming regions occurring within galaxies. So the bluer galaxies tend to have more star formation activities than redder galaxies.

Figure 4.6 is corresponding to the relation between $EW(H\alpha + [N\,II])$ and T-type. It is clearly seen that the $EW(H\alpha + [N\,II])$ tends to increase as a function of morphological types; the $EW(H\alpha + [N\,II])$ of late-type galaxies are much higher than early-types. The Sb galaxy (T-type = 3) has the highest $EW(H\alpha + [N\,II])$, equal to 15.577 Å. This indicates that star formation in late-type galaxies taking place more than the early-type galaxies, except for a Sm galaxy with S/N less than 3, which show a low $EW(H\alpha + [N\,II])$ of 1.247 Å. This is probably a result of morphological falsity and low S/N of $H\alpha$ flux counts.

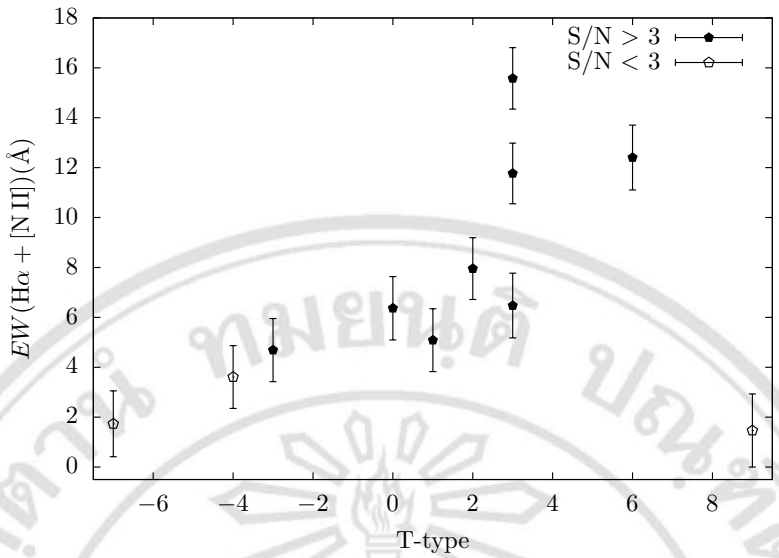

Figure 4.6: Distribution of Hα + [N II] emission equivalent width as a function of T-types.

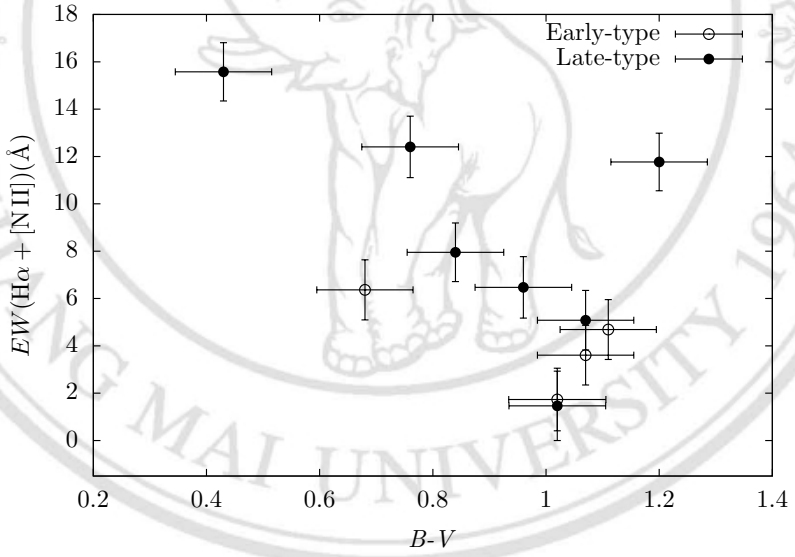

Figure 4.7: The diagram of Hα + [N II] emission equivalent width against color indices, separating with early-type and late-type.

The data points in figure 4.7 were separated to early-type (open circle) and late-type (filled circle) galaxies in order to compare with figure 4.5. James et al. (2004) suggested that the $EW(\mathrm{H}\alpha + [\mathrm{N\,II}])$ tends to increase and decrease as a function of morphological type and color, as shown in figure 4.6 and 4.7,respectively. Eventually, this indicates that star formation in bluer late-type galaxies taking place more than the redder early-type galaxies that is consistent with the previous research.

4.4 Mass of the Sample Galaxies

Mass of the sample galaxies was estimated by equation 3.41 in § 3.8.1. Figure 4.8 displays the distribution between the morphological types and mass of galaxies that were signified in term of $\log(M_{gal}/M_{\odot})$. An elliptical galaxy (E^{+}; T-type = -4) has the highest mass $2.775 \times 10^{12}\ M_{\odot}$. The lowest mass galaxy with mass $5.968 \times 10^{10}\ M_{\odot}$ is a dwarf elliptical galaxy (dE; T-type = -7). From this plot, it is consistent with Carroll and Ostlie (2014) who suggested the approximate range of the masses of galaxies. Mass of elliptical and spiral galaxies are in wild ranges of 10^{7} to $10^{13}\ M_{\odot}$ and 10^{9} to $10^{12}\ M_{\odot}$, respectively, while irregulars have masses ranging between 10^{8} and $10^{10}\ M_{\odot}$.

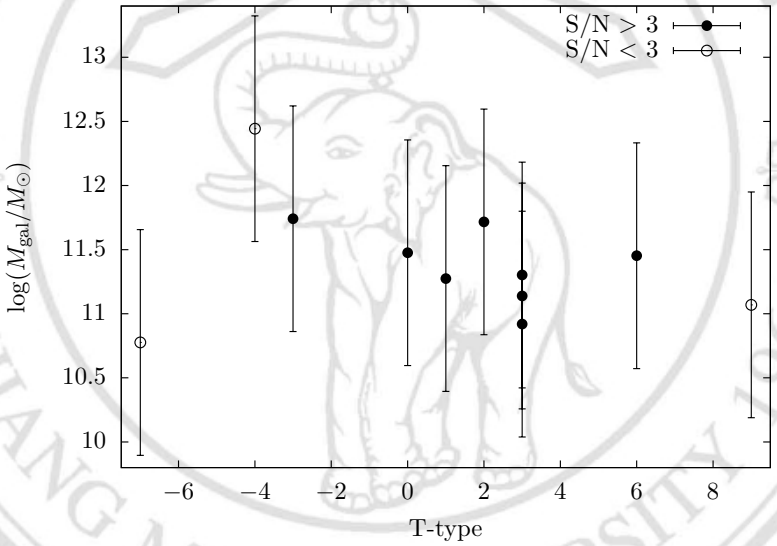

Figure 4.8: The distribution of $\log(M_{gal}/M_{\odot})$ against the T-types of sample galaxies.

4.5 Star Formation Rates

According to the [N II] corrected Hα flux counts in this research had been estimated by using two methods, i.e. methods of James et al. (2005) and Lee et al. (2009). Consequently, the Hα luminosities were calculated to approximate the SFR. The results are shown in table 3.13 and F.1. The two below plots are showing the SFR comparison between two methods. They can be interpreted that result difference is not very large, where the James et al. (2005) method has slightly larger SFR than the Lee et al. (2009) method. The cause of the difference came from the [N II] correction procedure for the Hα flux counts determination as presented in § 3.7.1.

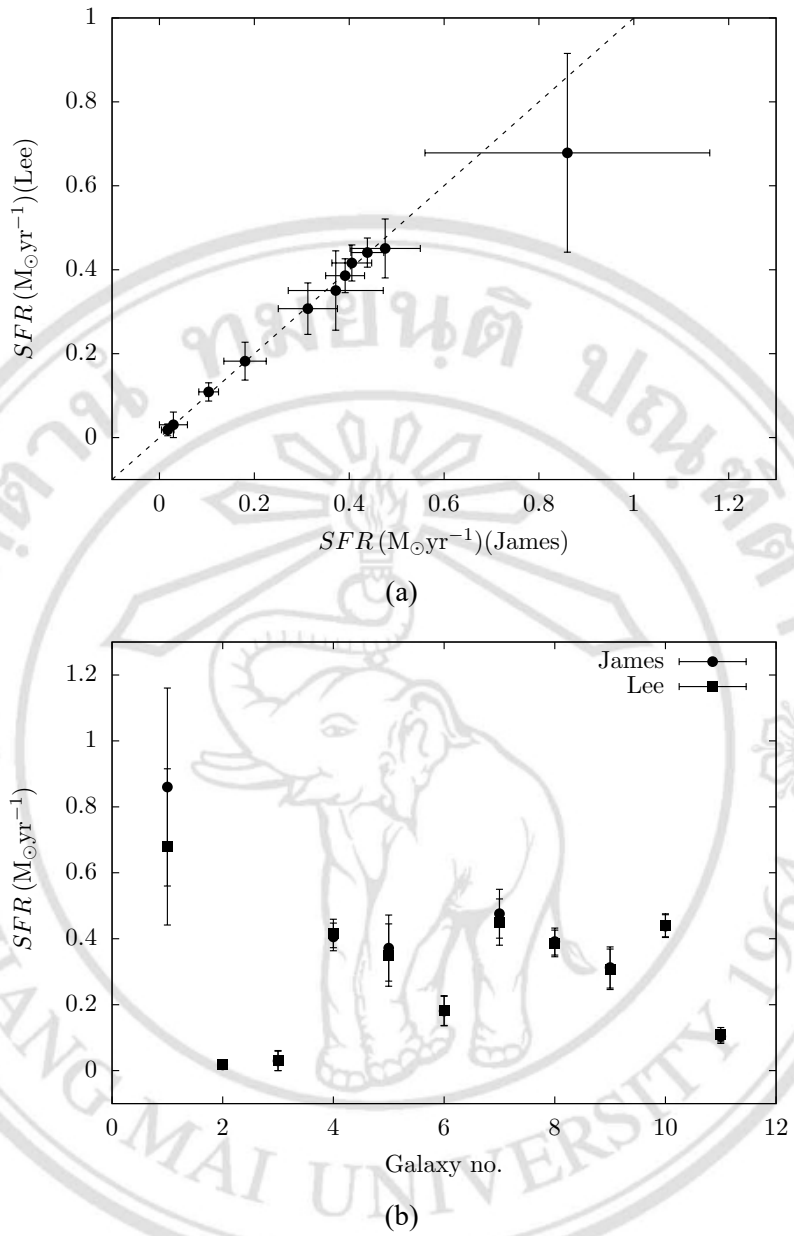

Figure 4.9: The comparison of star formation rate between two methods. A dash line in (a) represents the one to one line.

Kennicutt and Kent (1983) and Young et al. (1996) demonstrated that the measurement of $EW(\mathrm{H}\alpha)$ can be used to examine the star formation rate in galaxies. Figure 4.10 displays the correlation between SFR and $EW(\mathrm{H}\alpha)$. This study found that the SFR tends to increase with increasing $EW(\mathrm{H}\alpha)$ that is consistent with Koopmann et al. (2001), aside from a elliptical galaxy which appear high SFR, equal to 0.679 $\mathrm{M}_\odot\mathrm{yr}^{-1}$ with low $EW(\mathrm{H}\alpha)$, 2.343 Å. It may possibly have high surface brightness and emit the Hα fluxes more than the other galaxies, meanwhile it also emit high continuum fluxes (shown with

low S/N). When its $EW(\mathrm{H}\alpha)$ was calculated, it appeared smaller than most galaxies. However, the star formation rate per unit mass was mostly applied to compare the star formation activities in star-forming galaxies. Thus the mass of the galaxies that estimated in § 3.8.1 was used to normalize the SFR as listed in table 3.13, hereafter they were called

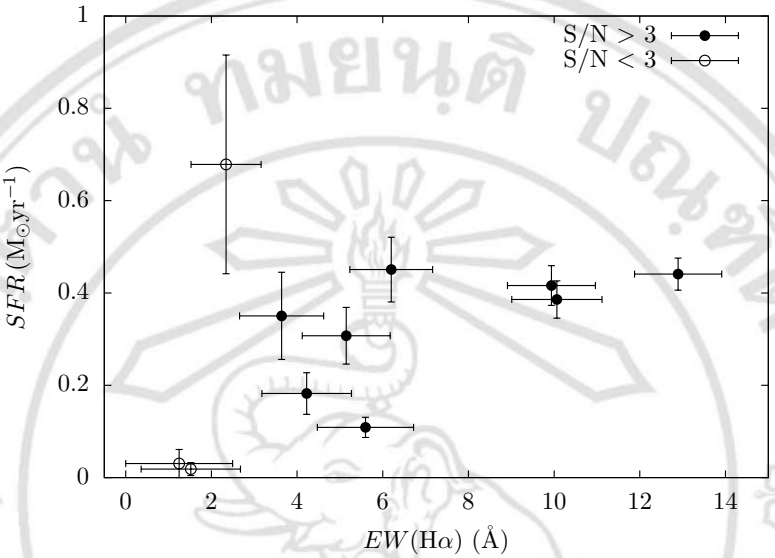

Figure 4.10: Distribution of star formation rate versus Hα equivalent width.

as normalized SFR ($nSFR$). After that, the physical parameters of the galaxies are plotted versus the star formation rate normalized by its mass. Figure 4.11 illustrates the distribution of $nSFR$ as a function of $B-V$ color. It is obviously seen that the bluer galaxies tend to have more $nSFR$ than redder galaxies, excluding for the most red ($B-V=$ 1.200) galaxy with highest $nSFR$, 3.023 $\times$ 10^{-12} yr^{-1}. As a result of this galaxy locates at the nearest from center of the galaxy group and is affected by the stronger tidal interaction than the other galaxies, which can trigger star formation efficiently.

The $nSFR$ was also distributed along the morphological T-types (see figure 4.12). It still increases with increasing T-type until type 3 (Sb or SBb), but the $nSFR$ surprisingly tends to be decreased with higher T-types (late-type of spirals to irregulars). The Sb sample galaxies in this research have the highest specific nSFR, that is 3.023 $\times$ 10^{-12} yr^{-1}. Because of Kennicutt (1983) and Gavazzi et al. (2002) who demonstrated that the $EW(\mathrm{H}\alpha)$ can be used as an effective probe of star-forming regions in the galaxies, the $nSFR$ and T-types distribution can be explained in the same way of figure 4.6.

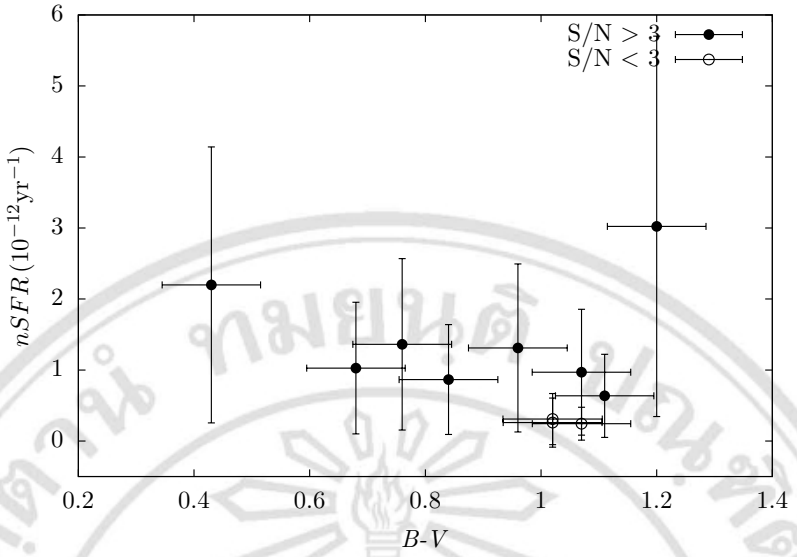

Figure 4.11: Distribution of the $nSFR$ against $B-V$ color index.

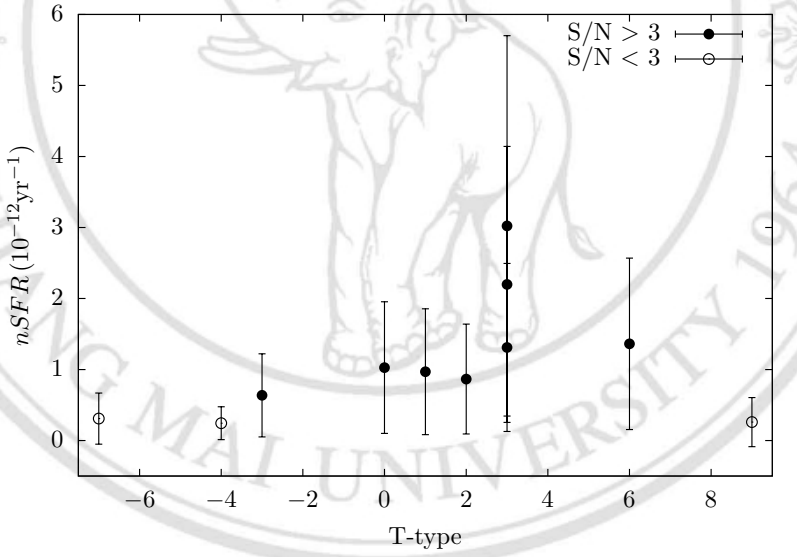

Figure 4.12: Distribution of the $nSFR$ against T-types.

Furthermore, the relation between the $nSFR$ against the $EW(\mathrm{H}\alpha)$ is illustrated in the figure 4.13. It is clearly seen that the $nSFR$ increases as a function of $EW(\mathrm{H}\alpha)$. This relation is consistent with the former study of Fossati et al. (2013) and Kennicutt (1998) that demonstrated that the measurement of $EW(H\alpha)$ could be a good indicator for star formation regions occurring within galaxies. The galaxies with $EW(\mathrm{H}\alpha)$ 9.937 Å has the highest $nSFR$ equal to $3.023 \times 10^{-12}\,\mathrm{yr}^{-1}$.

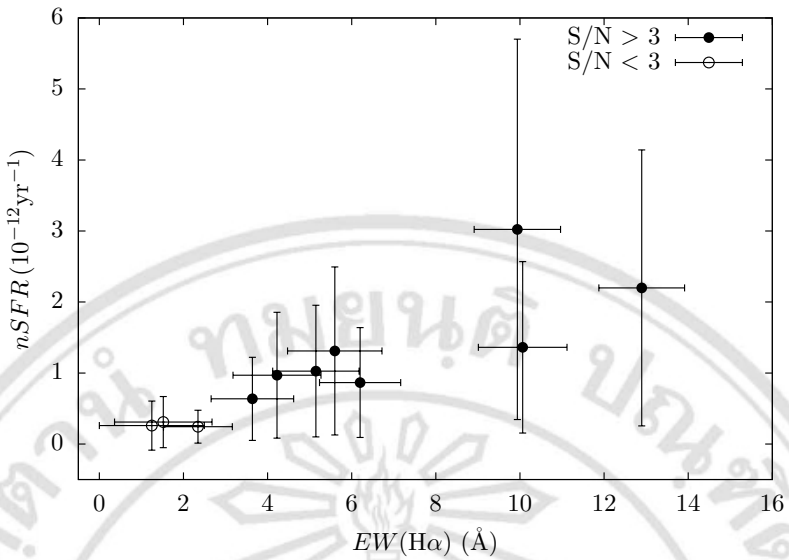

Figure 4.13: Distribution of the $nSFR$ against Hα equivalent width.

4.6 Perturbation Parameters of Tidal Interactions

This research has concentrated the tidal interactions between galaxy-galaxy and galaxy-group affect the star formation and evolution on the galaxy members of the galaxy group NGC 4213. Boselli and Gavazzi (2006) and Byrd and Valtonen (1990) provided the perturbation parameters to explain the efficiency of the tidal interactions. They can be determined by equation 3.48 for galaxy-galaxy interaction and equation 3.49 for galaxy-group interaction. r_{gal} in those equations represents the visual radius of the sample galaxies, which can be obtained from the relation between the angular size and averaged distance of galaxy group. Meanwhile R in equation 3.49 is the distance from galaxy to center of the galaxy group, that can be consolidated from the database, NED. Importantly, mass of the galaxy group is required to estimate the parameters. Thus the mass of the galaxy group was calculated by using virial theorem and we obtained 7.238×10^{13} $\mathrm{M}_{\odot}$ with bootstrapping uncertainty 3.727×10^{13} $\mathrm{M}_{\odot}$. The result of the galaxy-group perturbation parameters are given in a table 4.1. Since the critical value of the perturbation parameters are in range of $\geqslant$ 0.006 to 0.1 (Byrd and Valtonen, 1990). From this table, there are 8 galaxies that have individual parameter resided in the interval of critical values, where the highest value 0.3677 is belonged to 2MASX J12152202+2359376. So these galaxies will be

significantly disturbed and stimulated the star formation including morphological transformation simultaneously (Boselli and Gavazzi, 2006). Otherwise three galaxies which have the parameter value out of critical range might not be perturbed from the interaction because they locate too far from the center of galaxy group.

Table 4.1: The perturbation parameters of galaxy-group interactions.

Galaxy No.	Galaxy Names	P_{gc}	$\sigma_{P_{gc}}$
1	NGC 4213	0.0159	0.0141
2	2MASX J12154304+2400156	0.0085	0.0075
3	2MASX J12153399+2400116	0.0192	0.0169
4	2MASX J12152202+2359376	0.3677	0.3245
5	IC 0772	0.0912	0.0805
6	2MASX J12152523+2356536	0.0185	0.0163
7	UGC 07266	0.0447	0.0394
8	KUG 1212+241	0.0041	0.0036
9	2MFGC 09641	0.0223	0.0196
10	2MASX J12145681+2352066	0.0046	0.0041
11	2MASX J12155377+2356477	0.0020	0.0018

Table 4.2 shows the perturbation parameters of galaxy-galaxy interactions. A numerical data in each row represents the parameter that corresponds to the efficiency of perturbation occurred in the galaxy of that row by the neighbor galaxies which listed in each column. Such as the parameter 0.0016 will be used to describe the perturbation act on the galaxy no.1 by galaxy no.7 and so on. From the critical value, it was found that there are only 3 values show the relatively perturbation, i.e. 0.0246 for no.2 acts on no.1, 0.0340 for no.3 acts on no.1, and 0.0095 for no.4 acts on no.1. But entire other values are very tiny and out of critical range.

Table 4.2: The perturbation parameters of galaxy-galaxy interactions.

Galaxy No.	1	2	3	4	5	6	7	8	9	10	11
1	-	0.0246	0.0400	0.0095	0.0011	0.0025	0.0016	0.0001	0.0002	0.0001	0.0013
2	0.0007	-	0.0003	0.0001	0.0000	0.0000	0.0000	0.0000	0.0000	0.0000	0.0000
3	0.0023	0.0007	-	0.0007	0.0001	0.0001	0.0001	0.0000	0.0000	0.0000	0.0000
4	0.0002	0.0001	0.0003	-	0.0004	0.0002	0.0001	0.0000	0.0000	0.0000	0.0000
5	0.0003	0.0001	0.0002	0.0053	-	0.0019	0.0002	0.0000	0.0003	0.0001	0.0000
6	0.0003	0.0001	0.0002	0.0013	0.0009	-	0.0001	0.0000	0.0000	0.0000	0.0000
7	0.0001	0.0001	0.0002	0.0004	0.0000	0.0000	-	0.0000	0.0000	0.0000	0.0000
8	0.0000	0.0000	0.0000	0.0000	0.0000	0.0000	0.0000	-	0.0006	0.0003	0.0000
9	0.0000	0.0000	0.0000	0.0001	0.0001	0.0000	0.0000	0.0004	-	0.0008	0.0000
10	0.0000	0.0000	0.0000	0.0000	0.0000	0.0000	0.0000	0.0003	0.0014	-	0.0000
11	0.0001	0.0001	0.0000	0.0000	0.0000	0.0000	0.0000	0.0000	0.0000	0.0000	-